Ultrasonics 134 (2023) 107087

Contents lists available at ScienceDirect

Ultrasonics

journal homepage: www.elsevier.com/locate/ultras

Power-controlled acoustofluidic manipulation of microparticles

Fangda Wu [a], Hanlin Wang [a], Chao Sun [b], Fan Yuan [c], Zhihua Xie [d], Roman Mikhaylov [a], Zhenlin Wu [e], Minghong Shen [f], Jian Yang [f], Will Evans [a], YongQing Fu [g], Liangfei Tian [h], Xin Yang [a,*]

[a] Department of Electrical and Electronic Engineering, School of Engineering, Cardiff University, Cardiff CF24 3AA, UK
[b] School of Life Sciences, Northwestern Polytechnical University, 710072, PR China
[c] Department of Biomedical Engineering, School of Engineering, Duke University, NC 27708-0281, USA
[d] Department of Civil Engineering, School of Engineering, Cardiff University, Cardiff CF24 3AA, UK
[e] School of Optoelectronic Engineering and Instrumentation Science, Dalian University of Technology, 116023, PR China
[f] Division of Cancer and Genetics, School of Medicine, Cardiff University CF14 4XN, UK
[g] Faculty of Engineering and Environment, Northumbria University, Newcastle Upon Tyne, Newcastle NE1 8ST, UK
[h] College of Biomedical Engineering and Instrument Science, Zhejiang University, 310027, PR China

ARTICLE INFO

Keywords:
Acoustofluidics
Numerical simulations
Microparticles manipulations
Microchannel

ABSTRACT

Recently, surface acoustic wave (SAW) based acoustofluidic separation of microparticles and cells has attracted increasing interest due to accuracy and biocompatibility. Precise control of the input power of acoustofluidic devices is essential for generating optimum acoustic radiation force to manipulate microparticles given their various parameters including size, density, compressibility, and moving velocity. In this work, an acoustophoretic system is developed by employing SAW based interdigital electrode devices. Power meters are applied to closely monitor the incident and reflected powers of the SAW device, which are associated with the separation efficiency. There exists a range of input powers to migrate the microparticles to the pressure node due to their random locations when entering the SAW field. Theoretical analysis is performed to predict a proper input power to separate mixtures of polystyrene microspheres, and the end lateral position of microspheres being acoustically separated. The separation efficiency of four sizes of microspheres, including 20 μm, 15 μm, 10 μm, and 5 μm, is calculated and compared with experimental results, which suggest the input power for separating the mixture of these microspheres. The study provides a practical guidance on operating SAW devices for bioparticle separation using the incident power as a control parameter.

1. Introduction

Acoustofluidic devices have great advantages in the manipulation of biological particles such as circulating tumour cells (CTCs) [1–3], extracellular vesicles (EVs) [4,5], bacteria [6–8], and inflammatory cells [9]. Surface acoustic wave (SAW)-based acoustofluidic devices are increasingly used for cell manipulations with the benefit of contact-free, biocompatibility [10] and preserving the original cellular structure and states [3,11]. A typical structure of an acoustofluidic device consists of a SAW transducer made by a piezoelectric substrate and a microfluidic channel made by polydimethylsiloxane (PDMS). The acoustic radiation force on microparticles induced by SAW is determined by their size, density, and compressibility [12].

In the acoustofluidic device for cell separation, the deflection of microparticles is driven by the acoustic radiation force, which is associated with the input power of the device [13]. By tuning the input power from 60 to 82 mW, a travelling SAW device demonstrated separation of 15.2 μm microparticles from 10.2 μm and 19.5 μm, and 10.2 μm microparticles from 8.0 μm and 11.8 μm [14]. Another focused travelling SAW device was also capable of precisely actuating 2 μm microparticles by using the input power up to 100 mW [15]. Standing SAW (SSAW) devices were also applied to filtrate 8 μm microparticles from 5 μm, and separate 10.36 μm microparticles from 7.0 μm and 5.0 μm by controlling the input power [16]. For nanoparticles, tilted-angle SSAW devices were reported to achieve a deflection of particles of sizes from 220 nm to 900 nm with the corresponding input power from 0.5 W to 1.41 W [14].

As to the precisely power-controlled based acoustofluidic

* Corresponding author.
E-mail address: yangx26@cardiff.ac.uk (X. Yang).

https://doi.org/10.1016/j.ultras.2023.107087
Received 18 September 2022; Received in revised form 10 June 2023; Accepted 17 June 2023
Available online 19 June 2023

application, acoustofluidic sorting combined with fluorescence detector offers high-quality and automated isolation of cell subpopulations [17–19]. Microparticle and cell sorting using SAW has achieved very high throughput with the sample flow rate up to 500 μL/min [20]. On-chip single and double layer Hela cells coating [21] based on SSAW was effectively achieved, which enabled variable applications in chemistry, engineering, and medicine. Furthermore, acoustofluidic cell washing reduced cell damage caused by high shear stress in conventional centrifugation [22]. A comprehensive investigation between devices input power and separation efficiency will provide value guidance for acoustophoresis.

Given the acoustofluidic manipulation of microparticles has great potential in biomedical and chemical fields, better understanding of power-control manipulation will play key roles in improving separation efficiency. In this work, The control of the input power of SAW devices is investigated in association with microparticle separation efficiency. The theoretical calculation is also applied to predict the separation results of four microparticle sizes, including 5 μm, 10 μm, 15 μm, and 20 μm, which is compared with the experimental work.

2. Methodology

2.1. Mechanism of size-based acoustic separation

To investigate the quantitative relationship between the input power and separation efficiency, and to compare the result with theoretical estimation, an acoustofluidic device with three inlets and three outlets as shown in Fig. 1a & c was fabricated. The device consists of a pair of interdigital transducers (IDTs) by patterning gold electrodes on a piezoelectric substrate ($LiNbO_3$), and a PDMS microchannel. The microchannel was bonded on the $LiNbO_3$ between the IDTs with six polytetrafluoroethylene (PTFE) tubes connected to the ports. Both IDTs were driven by the same radio frequency (RF) signal to produce Rayleigh waves counter-propagating on the surface of the $LiNbO_3$ to form SSAW. The SSAW exhibited a series of locations at which the amplitude is zero or maximum, these locations were named pressure nodes (PNs) or pressure antinodes (ANs), respectively. The microchannel's width approximates half of the acoustic wavelength, which allows two PNs positioned near the two microchannel walls while an AN formed at the centre. A sample containing microparticles is introduced from the sample inlet. Two sheath flows are used to control the microparticle sample width and lateral position when entering the acoustic field via setting the flow rate ratio between the sheath and sample.

As the cross view of the model shown in Fig. 1b, the Rayleigh wave generated by the IDTs moves in an elliptical motion, producing both a vertical and horizontal component of motion in the direction of wave propagation. The displacement amplitude decays into the material so that they are mainly confined to within roughly one wavelength of the surface. Underneath a liquid inside a microchannel, the Rayleigh wave turns into a leaky Rayleigh wave, radiating pressure waves at the Rayleigh angle into the fluid, which presents an oscillatory acoustic field in the microchannel leading to time-averaged second-order effects. These effects are the main cause for the fluid and particle behaviour. Owing to viscous attenuation of the acoustic waves, a steady acoustic streaming flow $\boldsymbol{v}_{str}$ is formed. The $\boldsymbol{v}_{str}$ acts on suspended particles via the viscous drag force, $\boldsymbol{F}^{drag}$, in addition, they are also subject to the primary radiation force, $\boldsymbol{F}^{rad}$, due to wave scattering at the particle-liquid interfaces. The $\boldsymbol{F}^{rad}$ drives microparticles towards the PNs or ANs, depending on the sign of the acoustic contrast factor $\phi(\rho,\beta)$ ($\phi > 0$: moving towards PNs, $\phi<0$: moving towards ANs). The detailed mathematical derivation of the $\boldsymbol{F}^{rad}$ and the particle velocity can be found in the SI.

2.2. Device fabrication

The finger electrodes on the SAW device were patterned by evaporating a layer of 20-nm chrome and then 100-nm gold on the $LiNbO_3$ substrate (128° Y-cut, 0.5 mm thick and double-side polished). There were 40 pairs of finger electrodes on each IDT with the finger width, length, and pitch of 50 μm, 1 cm, and 100 μm, respectively. The distance between the centre of microchannel and the first front finger on both IDTs was 3 mm. The working frequency of the IDT was 19.6 MHz identified by sweeping frequency on a signal generator, which produces a SAW wavelength of 200 μm. When modelling the acoustic radiation force with the acoustic wavelength of 200 μm, Gor'kov's acoustic potential approach is valid for particle size not greater than 20 μm [23], which determines the maximum size of the microspheres used in this study.

The PDMS microchannel was made by pouring the mixture of silicon

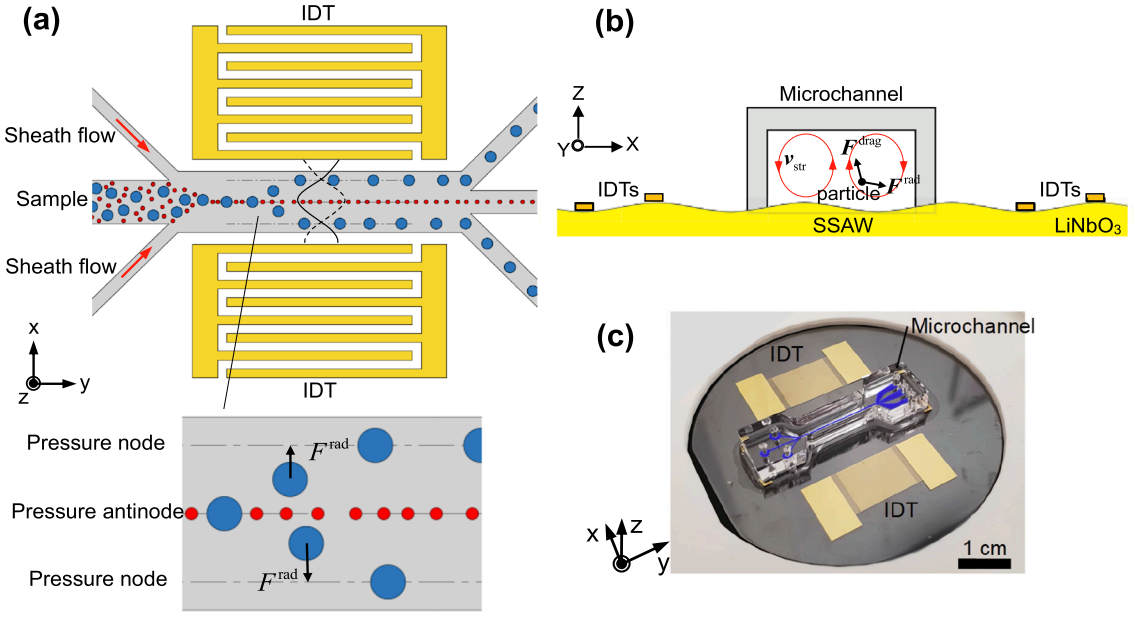

Fig. 1. (a) Schematic illustration of the standing surface acoustic wave (SSAW) device integrating two interdigital transducers (IDTs) and a microfluidic channel. (b) The net force exerted on the microparticle inside the acoustic microchannel is the combination of the acoustic radiation force $\boldsymbol{F}^{rad}$ and Stokes drag force $\boldsymbol{F}^{drag}$. (c) Photography of the SSAW device.

elastomer (DOWSIL, SYLGARD 184) and curing agent (DOWSIL, RT Cure) at the ratio of 10:1 (w/w) to an SU-8 mould, and then cured at 65 °C on a hotplate overnight. The widths of the microchannel inlet, outlet, and height were 100 μm, 80 μm, and 60 μm, respectively. The width of the middle part (acoustic active area) of the microchannel was 120 μm. The width of the outlet channel increased to 200 μm at the reservoir in order to stabilise the flow. A 0.5-mm punch was used to make ports for connecting the tubing on the PDMS microchannel. A droplet of isopropyl alcohol (IPA, Sigma-Aldrich, 2-Propanol solution) was applied between the surface of the IDT and the PDMS microchannel to avoid the friction during the alignment. The bonding was finished off by using a plasma treatment.

2.3. Polystyrene microspheres sample preparation

Four sizes of polystyrene microsphere including 5 μm, 10 μm, 15 μm, and 20 μm were prepared in a mixture of phosphate buffered saline (PBS) and glycerol (38:11, v/v). This ratio was used to mimic the density and viscosity of human whole blood. The glycerol could also prevent microsphere sedimentation. In the microsphere experiment, the concentration of the four microsphere sizes were 2×10^7, 1×10^7, 5×10^6, and 5×10^6 per mL, respectively. Smaller sizes were prepared at higher concentration to show a clear trajectory during the acoustic manipulation under the microscope. For the experiment separating one size from another, the smaller microspheres were diluted to approximately 1.5×10^6 per mL, and the bigger ones were diluted to approximately 7×10^5 per mL in each test group.

2.4. Experimental setup

The block diagram of the system set-up is shown in Fig. 2. A 19.6-MHz RF signal generated from the signal generator was amplified by a power amplifier (ZHL-100W-GAN+, Mini Circuits) and then divided equally by a power splitter (ZA2CS-251-20WS+, Mini Circuits) to drive the two IDTs. Power metres (8990B, Keysight) were applied to monitor the incident and reflected powers. The difference between the incident and reflected powers was calculated to determine the effective input power P_{in}, thus the acoustic pressure is given by (details in Eq. (S15), SI),

$$p_0 = \sqrt{\alpha \frac{(P_f - P_r)\rho_s c_s}{A_w}} \tag{1}$$

where P_f and P_r are the incident power and reflected powers, respectively, which were read using the two power meters connected to the couplers (ZFBDC20-62HP-S+, Mini Circuits). α is the power conversion efficiency, or electric-acoustic conversion factor, which determines the efficiency when the electrical energy converts to the acoustic energy via the IDT. The α represents the efficiency of energy conversion and affects the $\boldsymbol{F}^{rad}$ via acoustic pressure (details in the SI).

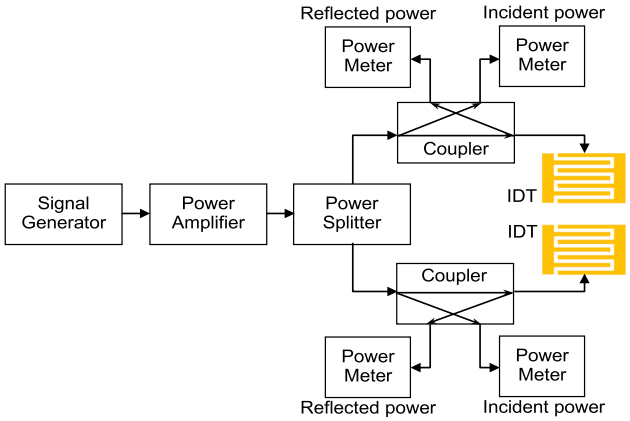

Fig. 2. System setup of the power-controlled SSAW separation.

A pressure pump (MK3+, EverFlow) was used to introduce the sample and two sheath flows (22% glycerol with 78% PBS) to the acoustofluidic device. Before each experiment, IPA, 0.1% bovine serum albumin (Sigma-Aldrich,) and PBS were used to flush the microchannel for approximately 30 min to remove any air bubbles and coat the microchannel. A haemocytometer was used to measure the concentration and the size of the sample before and after acoustic separation to calculate the separation efficiency by,

$$\frac{\#insheathoutlets}{\#incentreoutlet + \#insheathoutlets} = Seperationefficiency \tag{2}$$

In the experiment, 20 μm microspheres were firstly used to investigate the input power for microsphere translation, followed by the microspheres with other sizes. Microsphere sample was introduced to the acoustofluidic device by the pressure pump at a flow rate of 5 μL / min. The input power was increased from zero until almost full translation was achieved. The two sheath flows at 15 μL/ min were applied to create the sample width of 17 μm. Then microsphere mixtures of different sizes were introduced to the microchannel using the same sample and sheath flow rates.

3. Results and discussion

3.1. Analytical modelling of the acoustic separation

We set up an analytical model for determining the final position of the microspheres after acoustic separation. The acoustic radiation force and the separation efficiency were calculated using the theory given in the SI. The following computations were done in Matlab. Fig. 3a shows the schematic of the model, in which a sheath to sample flow rate ratio of 3:1 is set to focus the sample width to be 17 μm (yellow area), or ± 8.5 μm off the AN. The two PNs locate at the position ± 50 μm off the AN. In the acoustic field, microspheres are driven by the acoustic radiation force towards the PNs, where they are 'trapped' and flushed by the sheath flow to be collected at the side outlets. When the microsphere enters the acoustic field, its initial position, x_0, the distance from the AN, is randomly located within the sample width (yellow area), which determines its initial acoustic radiation force (Eq. (S13)). Its final position, x_f, is the distance from the AN to the microsphere end position.

Fig. 4 shows the calculation of the final position of the four sizes of microspheres with varying input powers. The vertical axis is the final

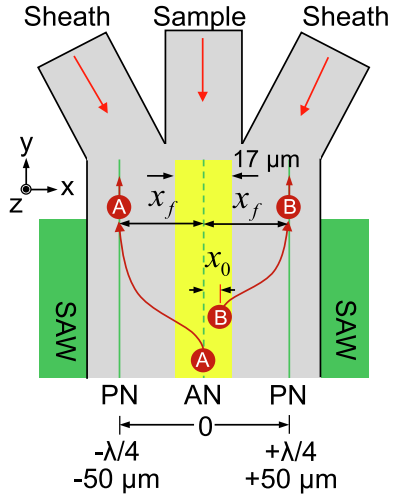

Fig. 3. The model of the acoustic separation. Two pressure nodes (PNs, green solid lines) are positioned near the wall of the microfluidic channel which attract microspheres to translate to the sides. AN is the pressure anti-node (green dash line). The yellow area is the sample width of 17 μm.

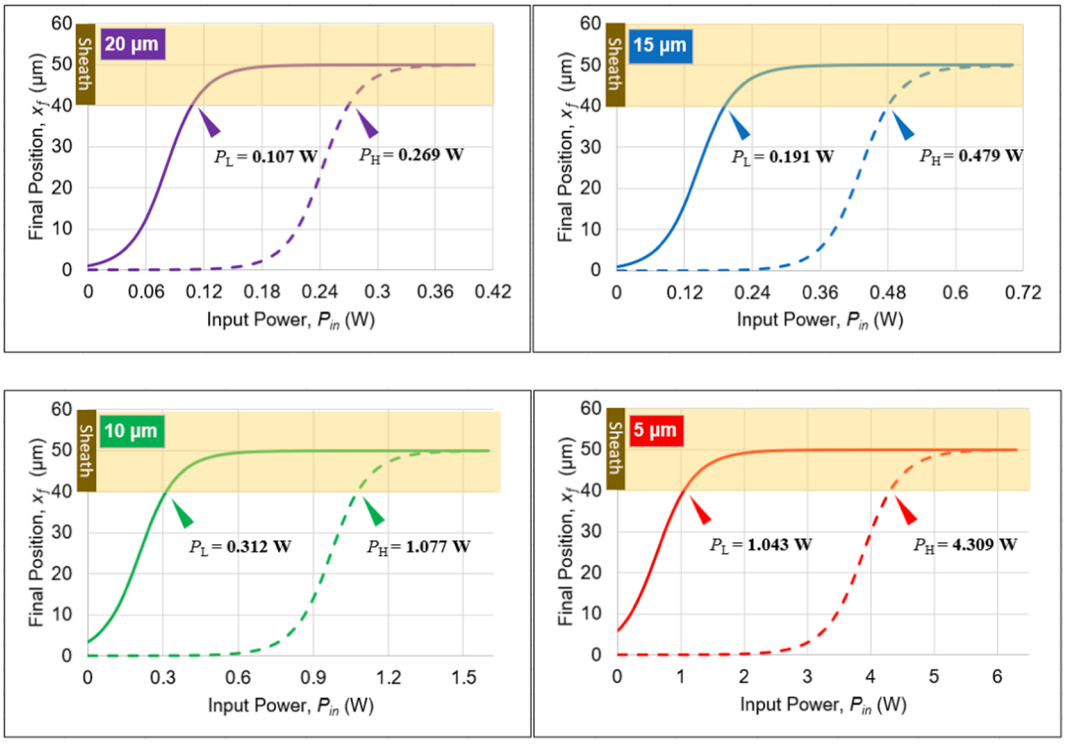

Fig. 4. Calculation of the final position for the four sizes of microspheres in the acoustofluidic device under different input powers. The upper power P_H is for translating microspheres close to the centre (AN), the lower power P_L is for translating microspheres at the boundary of the sample width.

position x_f of the microspheres inside the microchannel calculated by Eq. (S21). Solid lines show the final position of the microspheres which initiated from the sample flow (e.g. microsphere B in Fig. 3), while dash lines show the final position of the microspheres whose initial positions are slightly off the AN (e.g. microsphere A in Fig. 3). Thus, an upper power P_H and a lower power P_L are identified which are able to successfully translate microspheres across different lateral position in the sample width. The fluid velocity was considered as constant across the channel width due to small variation in velocity. The detailed description is given by Eqs. (S19) and (S20) in the SI.

The input power ranged between P_H and P_L for the four sizes of microspheres are shown in Fig. 5. Smaller microspheres require higher input power to be translated to the sheath. The corresponding acoustic radiation forces are also provided in Fig. S2. It can be predicted that if the input power of one microsphere is distinct from that of another microsphere, in their mixture, by operating the input power of the larger microsphere, the large one can be translated to the sheath outlet while the small one remains untranslated at the centre outlet. This allows one microsphere to be separated from the other effectively. For example,

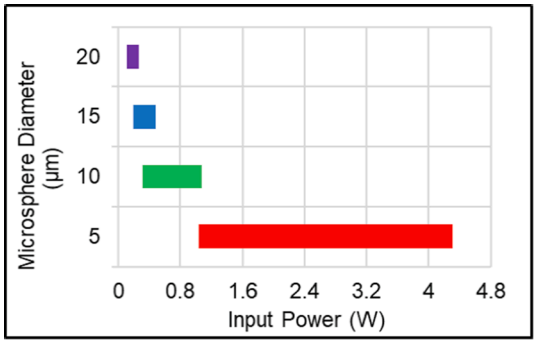

Fig. 5. Calculation of the range of the input power for translating the four sizes of microspheres from the sample to the sheath.

when operating the input power between 0.107 W and 0.269 W, 20 μm microspheres can be separated from the 10 μm ones.

A 90% separation efficiency, i.e. the number of microspheres collected from both sheath outlets accounts for 90% of the total number collected from both the sheath and centre outlets, is considered as a good separation rate[24]. To predict the separation efficiency, probability densities of microspheres at the inlet and outlet are analysed using the model detailed in the SI. The width of the sheath outlet is much greater than the microspheres, presence of the microspheres near the sheath outlet can guarantee being separated from the sample. In the modelling, as long as the particles entered the sheath outlet area (yellow regions in Figs. 4 & 6), they are considered to be "separated". At the inlet, all the microspheres are concentrated between ± 8.5 μm off the centre of the microchannel due to the focusing effect produced by the two sheath flows (dotted line in Fig. 6a). The microspheres are deflected by the acoustic field resulting in an increasing microsphere density at the sheath regions (solid line in Fig. 6a). When the input power is set to 0.564 W, 90% of the 10 μm microspheres are migrated to the sheath. The input power is altered in the model to investigate the power for separating microspheres with different sizes. Fig. 6b shows a critical input power of 0.107 W, at which all the microspheres still stay in the centre without being translated to the sheath for collection, and the sample width of the 20 μm microspheres increases from 20 μm to 80 μm. Increasing the input power can further decrease the centre density and increase the sheath density. An example with the input power of 0.25 W is given in Fig. 6c in which neither 5 μm nor 10 μm microspheres receives sufficient acoustic radiation force to migrate to the sheath for the given separation length (1 cm, the same as the length of the IDT), while almost all the 20 μm microspheres translate to the sheath and 64.8% of the 15 μm microspheres are collected at the sheath outlet.

The above results indicate a clear relationship between the input power and the separation efficiency of different sizes of microspheres. Fig. 5 informs the feasibility to separate microspheres between 20 μm and 10 μm, 15 μm and 5 μm, which leads to Fig. 7 showing the theoretical input power to separate these two combinations and guiding the

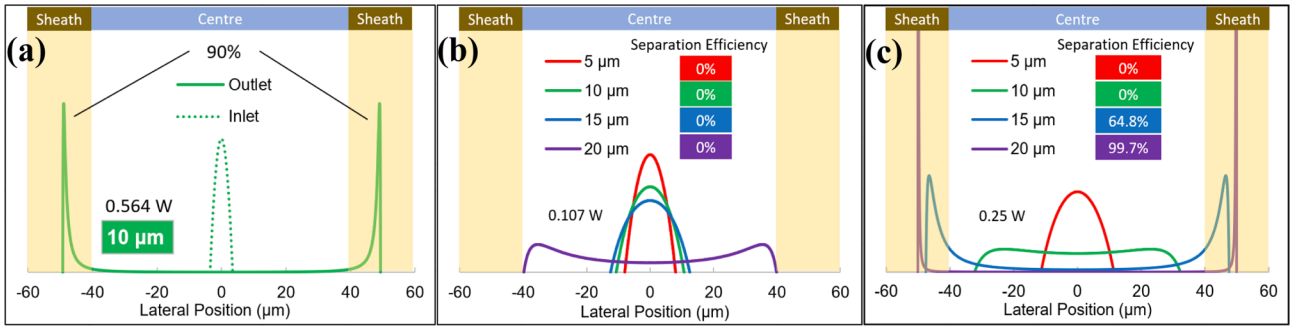

Fig. 6. Modelling the separation efficiency. (a) The probability density of the 10 μm microsphere at the inlet and outlet when the input power is 0.564 W. (b) The critical input power (0.107 W) to keep all microspheres remained at the centre. (c) When the input power is 0.25 W, nearly all the 20 μm microspheres are translated to the sheath, while the 64.8% of 15 μm microspheres are migrated to the sheath, both the 5 and 10 μm microspheres stay at the centre.

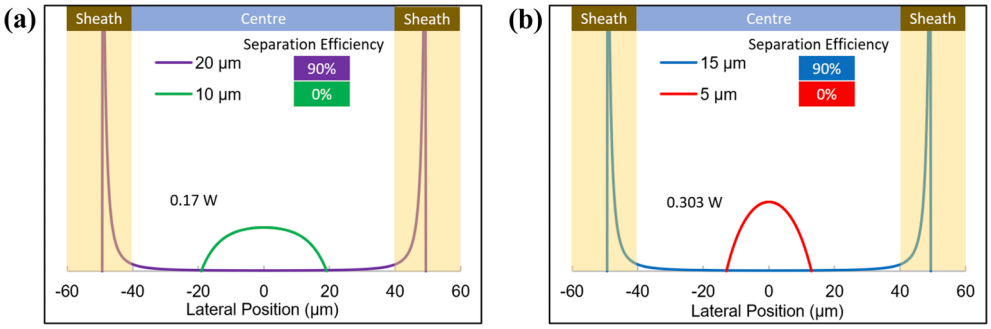

Fig. 7. Theoretical calculation of the separation efficiency. (a) The distribution of 20 μm and 10 μm microspheres after separation at the input power of 0.17 W. (b) The distribution of 15 μm and 5 μm microspheres after separation at the input power of 0.303 W.

following experiments to choose a suitable input power to achieve effective separation.

It is worth to note that the calculation neglects the secondary radiation force for the sake of calculation simplicity. In acoustofluidic field, the acoustic radiation force can be divided into two types, namely, primary radiation force experienced by single particles, which causes them to migrate towards PN or AN, and secondary radiation force responsible for particle–particle interactions [25], which makes them attract or repel one another, and sometimes form stable multi-particle structures.

3.2. Input powers

To investigate the effective input power of the IDTs, the incident power and the reflected powers were monitored by using the power meters. The output power of the signal generator was adjusted to produce an amplified output power between 0.3 W and 2 W, as shown in Fig. 8. The effective input power, P_{in}, is well correlated to the incident power, P_f. The power reflection from the IDTs is between 4% and 6%, which indicate a high energy conversion efficiency on both IDTs.

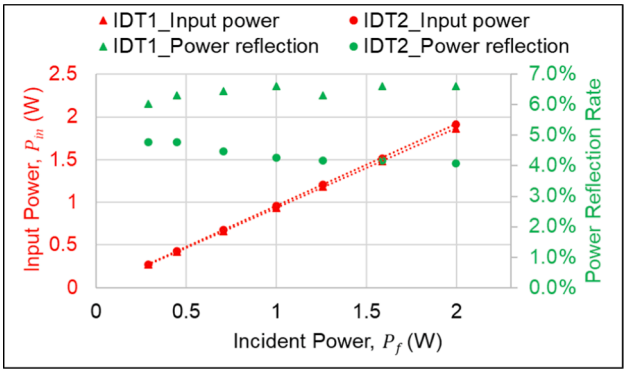

Fig. 8. The relationship between the effective input power and the incident power of both IDTs. The effective input power is calculated by subtracting the incident power by the reflected power.

3.3. The power to translate polystyrene microspheres

To validate the separation model, the following experiment was conducted to separate four sizes of microparticles as the results shown in Fig. 9. In general, the experimental data follows the theoretical calculation trend. The power to achieve 90% microsphere translation is generally larger than the theoretical calculation. This could be caused by the uneven distribution of particles in the sample flow before they flow into the SSAW field in the experiment. The current method provides an alternative technique to frequency modulation presented by [26], allowing effective separation to achieve by controlling the RF input power with simplicity in adjusting separation threshold.

By looking up the input powers in the experimental data corresponding to the separation efficiency of 90%, one can suggest a practical input power for separating the mixture of 20 μm and 10 μm, 15 μm and 5 μm, as given in Table 1.

3.4. The power to separate polystyrene microsphere mixture

Fig. 10 shows the separation efficiency of the two microsphere mixtures. As shown in Fig. 10a, by adjusting the input power, 86% of 20 μm microspheres are separated at the input power of 0.22 W while 74% of 10 μm microspheres remain in the centre outlet. Fig. 10b shows 98% of 15 μm microspheres are separated from 5 μm at the input power of 0.4 W, achieving 89% of 5 μm microspheres in the centre outlet. The large error bars on the 20 μm microspheres could be caused by the collision of microspheres during the separation process.

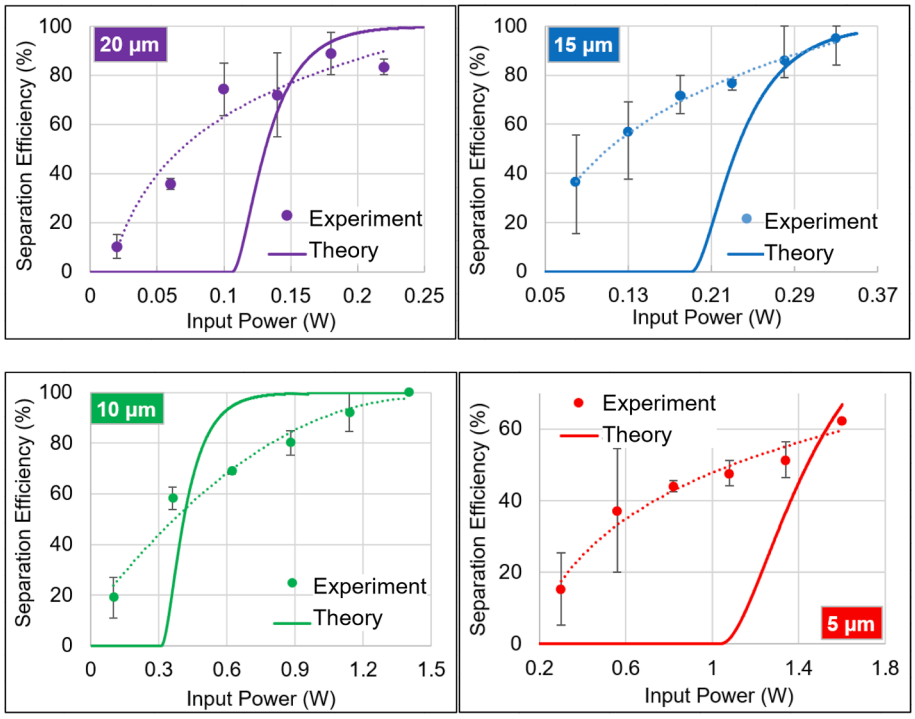

Fig. 9. The separation efficiency of the four sizes of microspheres in the acoustofluidic device under different input powers.

Table 1
The theoretical, experimentally predicted, and practical input powers to separate polystyrene microsphere mixture of 20 μm and 10 μm, 15 μm and 5 μm.

	20 μm and 10 μm mixture	15 μm and 5 μm mixture
Theoretically predicted input power	0.170 W	0.303 W
Experimentally predicted input power	0.221 W	0.302 W
Practical input power	0.252 W	0.301 W

Fig. 11a & 11b are the example microscopic images showing the mixture of 20 μm and 10 μm microspheres when SAW is off and on, respectively. Both microspheres disperse evenly in the three outlet channels when SAW is off. During SAW is on, 20 μm microspheres migrate to the PNs located at the sheath while most 10 μm microspheres remain on the central course or move at a much slower velocity towards the PNs.

4. Conclusions

In this work, an SSAW-based acoustofluidic device was applied to investigate the relationship between the input power and microsphere separation efficiency. Polystyrene microspheres of 20 μm, 15 μm, 10 μm, and 5 μm were theoretically studied and applied in separation experiment. The input power of the device was associated with the separation efficiency and the distribution density inside the microfluidic channel. There existed an input power range to migrate the microparticle across the sample width. Our model provided a tool to determine the input power to separate microparticles with different sizes. The experimental separation efficiency of 5 μm, 10 μm, 15 μm, and 20 μm was in good agreement with the theoretical prediction.

Declaration of Competing Interest

The authors declare that they have no known competing financial interests or personal relationships that could have appeared to influence the work reported in this paper.

Data availability

No data was used for the research described in the article.

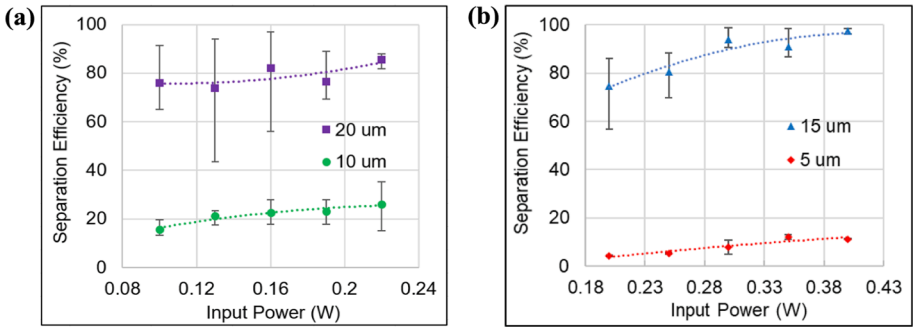

Fig. 10. Separation efficiencies of two mixtures of polystyrene microspheres. (a) 20 μm and 10 μm; (b) 15 μm and 5 μm.

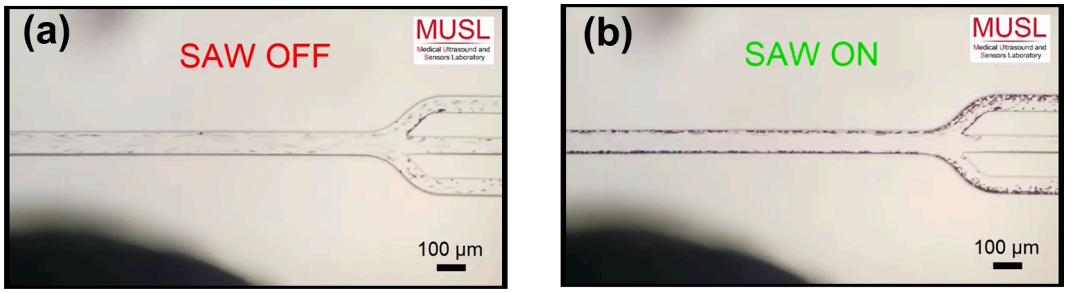

Fig. 11. Microscopic images of microsphere separation between 20 μm and 10 μm. (a) When SAW is off microspheres of 20 μm and 10 μm are found in all 3 outlets. (b) When SAW is on, 20 μm microspheres are separated and collected by the two side outlets.

Appendix A. Supplementary data

Supplementary data to this article can be found online at https://doi.org/10.1016/j.ultras.2023.107087.

References

[1] P. Li, et al., Acoustic separation of circulating tumor cells, Proc. Natl. Acad. Sci. 112 (16) (2015) 4970–4975.
[2] M. Antfolk, C. Magnusson, P. Augustsson, H. Lilja, T. Laurell, Acoustofluidic, label-free separation and simultaneous concentration of rare tumor cells from white blood cells, Anal. Chem. 87 (18) (2015/09/15 2015.) 9322–9328.
[3] M. Wu et al., Circulating tumor cell phenotyping via high-throughput acoustic separation, vol. 14, no. 32, p. 1801131, 2018.
[4] M. Wu et al., Isolation of exosomes from whole blood by integrating acoustics and microfluidics, p. 201709210, 2017.
[5] K. Lee, H. Shao, R. Weissleder, H. Lee, Acoustic purification of extracellular microvesicles, ACS Nano 9 (3) (2015/03/24 2015.) 2321–2327.
[6] P. Ohlsson, K. Petersson, P. Augustsson, T. Laurell, Acoustic impedance matched buffers enable separation of bacteria from blood cells at high cell concentrations, Sci. Rep. 8 (1) (2018/06/14 2018.) 9156.
[7] S. Li, F. Ma, H. Bachman, C.E. Cameron, X. Zeng, T.J. Huang, Acoustofluidic bacteria separation, J. Micromech. Microeng. : Struct. Devices Syst. 27 (1) (2017), 015031.
[8] P. Ohlsson, et al., Integrated acoustic separation, enrichment, and microchip polymerase chain reaction detection of bacteria from blood for rapid sepsis diagnostics, Anal. Chem. 88 (19) (2016/10/04 2016.) 9403–9411.
[9] S. Li, et al., Acoustofluidic transfer of inflammatory cells from human sputum samples, Anal. Chem. 88 (11) (2016/06/07 2016.) 5655–5661.
[10] P. Zhang, H. Bachman, A. Ozcelik, T.J. Huang, "Acoustic Microfluidics," (in eng), Annual Rev. Anal. Chem. (Palo Alto Calif.) 13 (1) (2020) 17–43.
[11] P. Augustsson, J.T. Karlsen, H.-W. Su, H. Bruus, J. Voldman, Iso-acoustic focusing of cells for size-insensitive acousto-mechanical phenotyping, Nat. Commun., Article vol. 7, p. 11556, 05/16/online 2016.
[12] H. Bruus, Acoustofluidics 1: Governing equations in microfluidics, Lab Chip, 10.1039/C1LC20658C vol. 11, no. 22, pp. 3742-3751, 2011.
[13] J. Shi, H. Huang, Z. Stratton, Y. Huang, T.J. Huang, Continuous particle separation in a microfluidic channelvia standing surface acoustic waves (SSAW), Lab Chip, 10.1039/B915113C vol. 9, no. 23, pp. 3354-3359, 2009.
[14] M. Wu, et al., Acoustic Separation of Nanoparticles in Continuous Flow 27 (14) (2017) 1606039.
[15] D.J. Collins, A. Neild, Y. Ai, Highly focused high-frequency travelling surface acoustic waves (SAW) for rapid single-particle sorting, Lab Chip, 10.1039/C5LC01335F vol. 16, no. 3, pp. 471-479, 2016.
[16] A. Fakhfouri, C. Devendran, D.J. Collins, Y. Ai, A. Neild, Virtual membrane for filtration of particles using surface acoustic waves (SAW), Lab Chip, 10.1039/C6LC00590J vol. 16, no. 18, pp. 3515-3523, 2016.
[17] A.A. Nawaz, et al., Acoustofluidic Fluorescence Activated Cell Sorter, Anal. Chem. 87 (24) (2015) 12051–12058.
[18] Z. Ma, Y. Zhou, D.J. Collins, Y. Ai, "Fluorescence activated cell sorting via a focused traveling surface acoustic beam," (in eng), Lab Chip 17 (18) (2017) 3176–3185.
[19] L. Ren, et al., Standing Surface Acoustic Wave (SSAW)-Based Fluorescence-Activated Cell Sorter, Small 14 (40) (2018) 1801996.
[20] M. Wu, et al., High-throughput cell focusing and separation via acoustofluidic tweezers, Lab Chip 18 (19) (2018) 3003–3010.
[21] B. Ayan, et al., Acoustofluidic coating of particles and cells, Lab Chip 16 (22) (2016) 4366–4372.
[22] S. Li, et al., Standing surface acoustic wave (SSAW)-based cell washing, Lab Chip, 10.1039/C4LC00903G vol. 15, no. 1, pp. 331-338, 2015.
[23] J.F. Pazos Ospina, V. Contreras, J. Estrada-Morales, D. Baresch, J.L. Ealo, K. Volke-Sepúlveda, Particle-size effect in airborne standing-wave acoustic levitation: trapping particles at pressure antinodes, Phys. Rev. Appl., vol. 18, no. 3, p. 034026, 09/12/ 2022.
[24] M. Wu, A. Ozcelik, J. Rufo, Z. Wang, R. Fang, T.J. Huang, Acoustofluidic separation of cells and particles, Microsyst. Nanoeng. 5 (1) (2019) 32.
[25] A. Doinikov, Acoustic radiation forces: Classical theory and recent advances, vol. 1, 2003, pp. 39-67.
[26] G. Simon, et al., Particle separation in surface acoustic wave microfluidic devices using reprogrammable, pseudo-standing waves, Appl. Phys. Lett. 113 (4) (2018/07/23 2018.), 044101.